Supporting Information

Optical properties of Nd^{3+} and Yb^{3+} -doped Ag*M*$(IO_3)_4$ metal iodates: transparent host matrices for mid-IR lasers and nonlinear materials.

Delphine Phanon [I], Yan Suffren [I], Mohamed B. Taouti [II], Djamal Benbertal [II], Alain Brenier [III], Isabelle Gautier-Luneau [I*]

[I] Université Grenoble Alpes, Institut NEEL, F-38042 Grenoble, France

[II] Université de Laghouat, Laboratoire de Physico-Chimie des Matériaux, BP 37G. Laghouat 03000, Algérie

[III] Institut Lumière Matière, UMR5306 Université Lyon 1-CNRS, Université de Lyon, 69622 Villeurbanne cedex, France

[*]Corresponding author: Isabelle.Gautier-Luneau@neel.cnrs.fr

Fax: +33 4 76 88 10 38; Tel: + 33 4 76 88 78 04

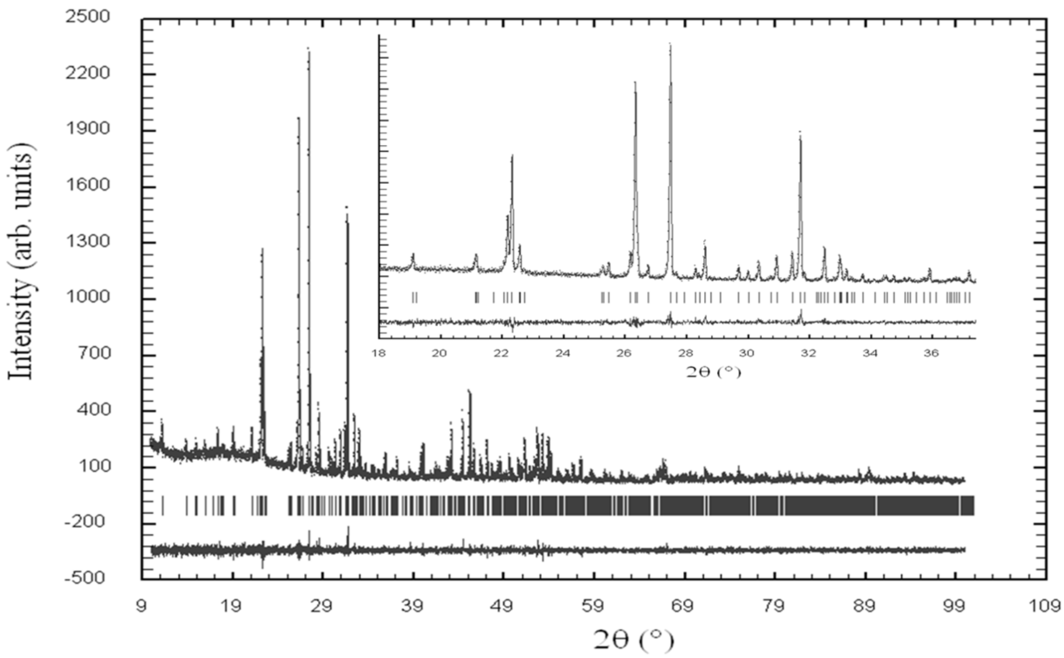

Figure S1. Observed (points), calculated (line) and difference (bottom line) X-ray diffraction pattern of $NaNd(IO_3)_4$ measured on D8 Bruker (λ = 1.54056 Å). Vertical lines indicate Bragg positions of the contribution phase $NaNd(IO_3)_4$.

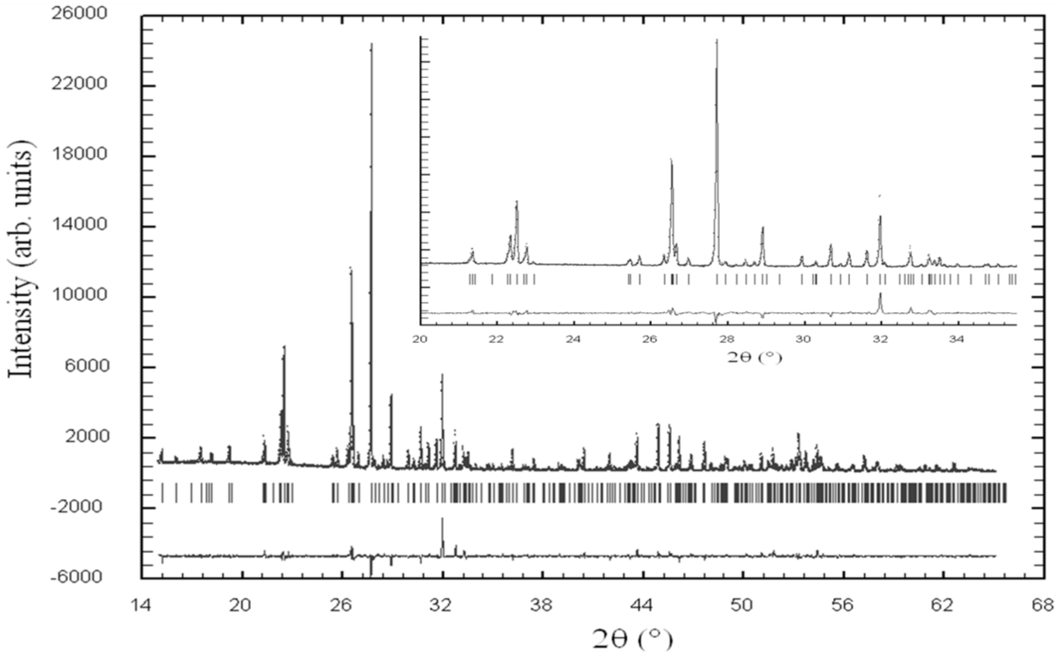

Figure S2. Observed (points), calculated (line) and difference (bottom line) X-ray diffraction pattern of $NaGd(IO_3)_4$ measured on D8 Bruker (λ = 1.54056 Å). Vertical lines indicate Bragg positions of the contribution phase $NaGd(IO_3)_4$.

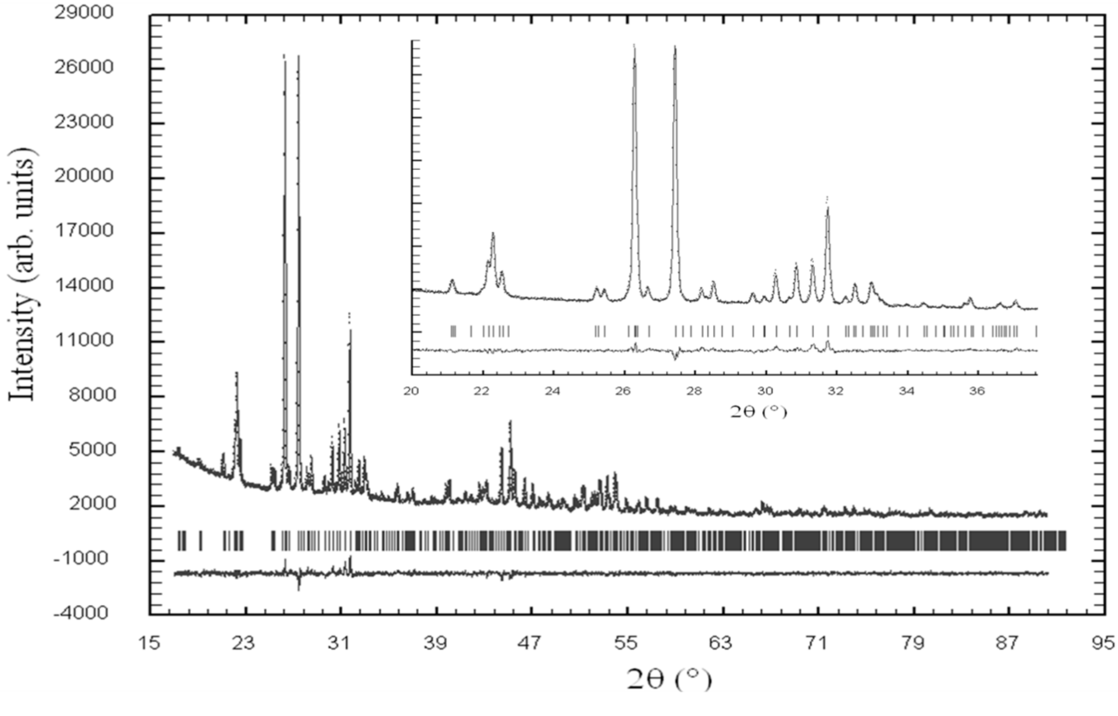

Figure S3. Observed (points), calculated (line) and difference (bottom line) X-ray diffraction pattern of $AgNd(IO_3)_4$ measured on D8 Bruker (λ = 1.54056 Å). Vertical lines indicate Bragg positions of the contribution phase $AgNd(IO_3)_4$.

Table S1 Coordination schemes of iodate anion towards cations in Na$M(IO_3)_4$, M=Y, Nd, Gd and Ag$M'(IO_3)_4$, M'= Y, La, Nd, Eu, Gd, Bi.

Iodate group	coordination schemes
$I(1)O_3$	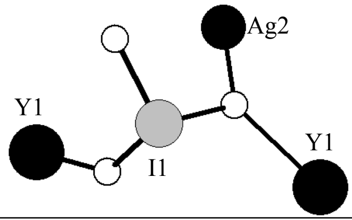
$I(2)O_3$ and $I(7)O_3$	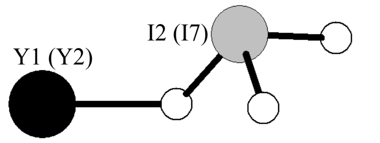
$I(3)O_3$ and $I(5)O_3$	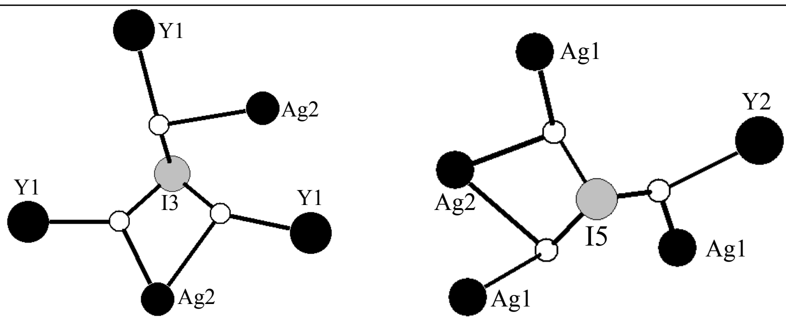
$I(4)O_3$	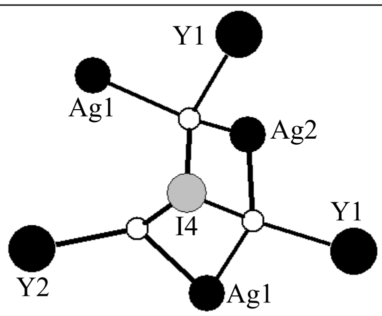
$I(6)O_3$	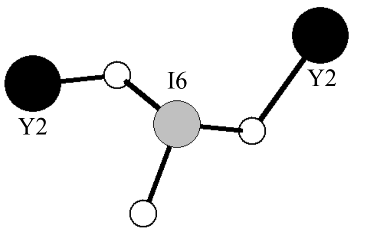
$I(8)O_3$	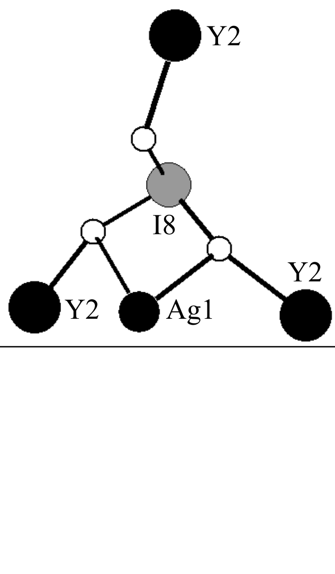

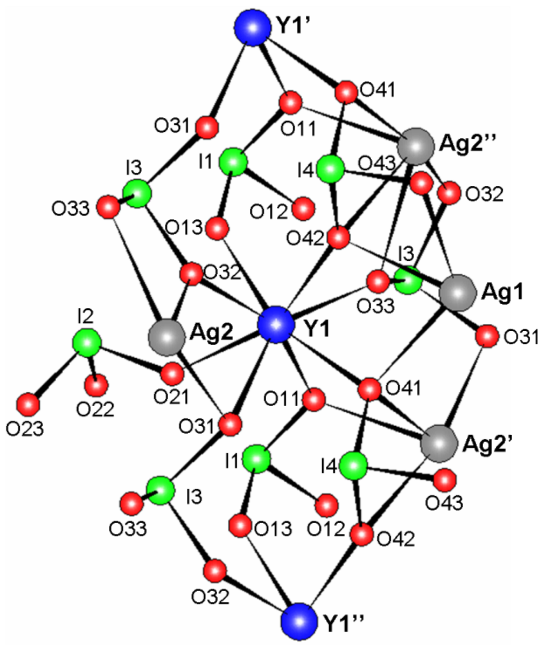

d(Y1…Ag1) = 3,952(7) Å
d(Y1…Ag2) = 3,939(7) Å
d(Y1…Ag2') = 3,820(7) Å
d(Y1…Ag2'') = 4,230(7) Å
d(Y1…Y1') = d(Y1…Y1'') = 5,547(7) Å (= *b*)

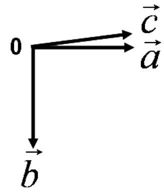

Figure S4 : Environment of Y1 in $AgY(IO_3)_4$ showing the nearest metal neighbors. Each $\{Y(1)O_8\}$ polyhedron is linked by edge-sharing to four metals (one Ag1 and three Ag3 atoms) and connected via (*M*-O-I-O-*M*) bridging to two Y1 atoms.

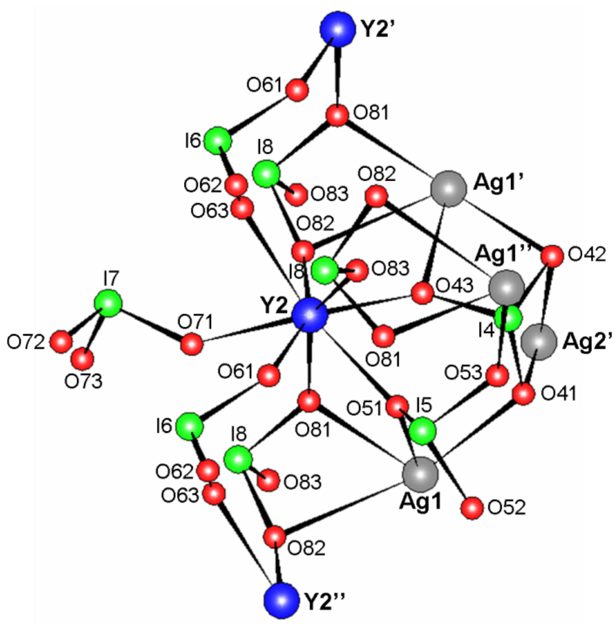

d(Y2…Ag1) = 4,156(7) Å
d(Y2…Ag1') = 4,274(7) Å
d(Y2…Ag1'') = 5,550(7) Å
d(Y2…Ag2') = 5,737(7) Å
d(Y2…Y2') = d(Y2…Y2'') = 5,547(7) Å (= *b*)

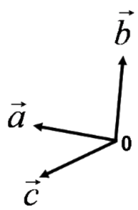

Figure S5 : Environment of Y2 in $AgY(IO_3)_4$ showing the nearest metal neighbors
Each $\{Y(2)O_8\}$ polyhedron is linked by edge-sharing to Ag1 atoms and connected via (*M*-O-I-O-*M*) bridging to four atoms (1 Ag1, 1 Ag2 and 2 Y2).

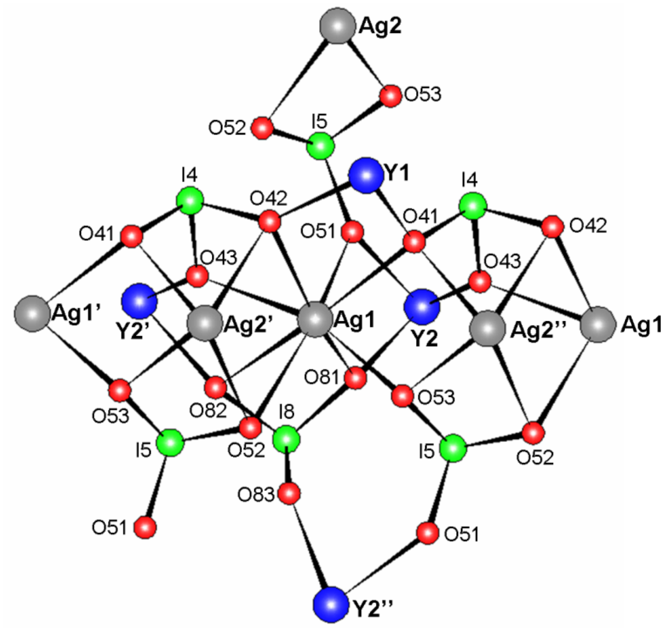

d(Ag1…Ag2’) = 3,678(7) Å
d(Ag1…Ag2’’) = 3,873(7) Å
d(Ag1…Y1) = 3,952(7) Å
d(Ag1…Y2) = 4,156(7) Å
d(Ag1…Y2’) = 4,274(7) Å
d(Ag1…Y2’’) = 5,550(7) Å
d(Ag1…Ag1’) = d(Ag1…Ag1’’) = 5,547(7) Å (= *b*)
d(Ag1…Ag2) = 5,656(7) Å

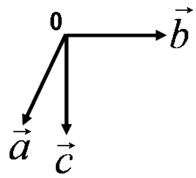

Figure S6 : Environment of Ag1 in $AgY(IO_3)_4$ showing the nearest metal neighbors. Each $\{Ag(1)O_8\}$ polyhedron is linked by edge-sharing to five metals: two Ag2, two Y2 and one Y1 atoms, and connected via (*M*-O-I-O-*M*) bridging to one Y1, two Ag1 and one Y2 atoms.

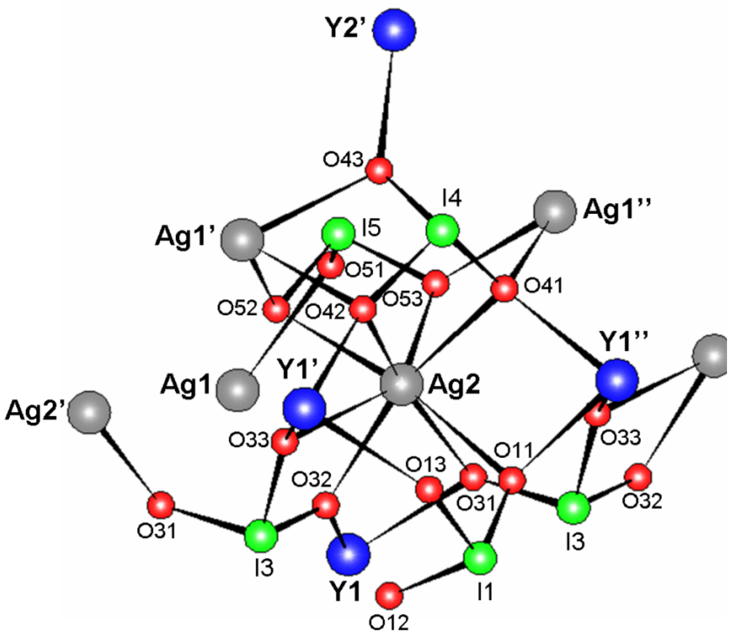

d(Ag2…Ag1’) = 3,678(7) Å
d(Ag2…Ag1’’) = 3,873(7) Å
d(Ag2…Y1) = 3,939(7) Å
d(Ag2…Y1’) = 4,230(7) Å
d(Ag2…Y1’’) = 3,820(7) Å
d(Ag2…Ag2’) = d(Ag2…Ag2’) =
5,547(7) Å (= *b*)
d(Ag2…Ag1) = 5,656(7) Å
d(Ag2…Y2’) = 5,737(7) Å

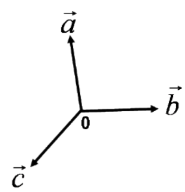

Figure S7 : Environment of Ag2 in $AgY(IO_3)_4$ showing the nearest metal neighbors. The $\{Ag(2)O_8\}$ polyhedron is linked by edge-sharing to three Y1 atoms and two Ag1 atoms, and connected via (*M*-O-I-O-*M*) bridging to one Ag1, two Ag2 and one Y2 atoms.

Thermal analyses: DSC analyses were carried out on a NETZSCH ATD-DSC 404S apparatus and ran in the range 25-700°C, in argon flow at 5°C/min heating rate. DSC curves of $NaY(IO_3)_4$, $AgY(IO_3)_4$, $AgBi(IO_3)_4$ and $AgLa(IO_3)_4$ are shown in Fig. 7a and b.

DSC curve of $NaY(IO_3)_4$ shows only one decomposition peak at 550°C. The residue has been identified as the cubic phase of Y_2O_3 (JCPDS file no.76-0151). No phase transition is observed before 550°C. Decomposition of $AgY(IO_3)_4$ is done in two steps. The first peak centred at 430°C corresponds to the formation of a new phase which has not been identified. The second peak at 550°C is due to a mixture of AgI (JCPDS file no.01-0502) and Y_2O_3 (JCPDS file no.76-0151 cubic phase). Studies lead in furnace, do not reveal phase transition before 430°C.

$AgBi(IO_3)_4$ also decays in two steps. The first peak at 490°C corresponds to the formation of a mixture of AgI (JCPDS file no.01-0502) and Bi_5O_7I (JCPDS file no.40-0548). At 540°C, residue has been identified as Bi_2O_3 (JCPDS file no.78-1793 tetragonal phase). No phase transition is observed before 490°C.

Decomposition of $AgLa(IO_3)_4$ is done in two step. The first peak at 500°C highlights the fusion of the compound. The second peak at 530°C shows the formation of a mixture of AgI and La_2O_3. No phase transition is observed before 500°C.

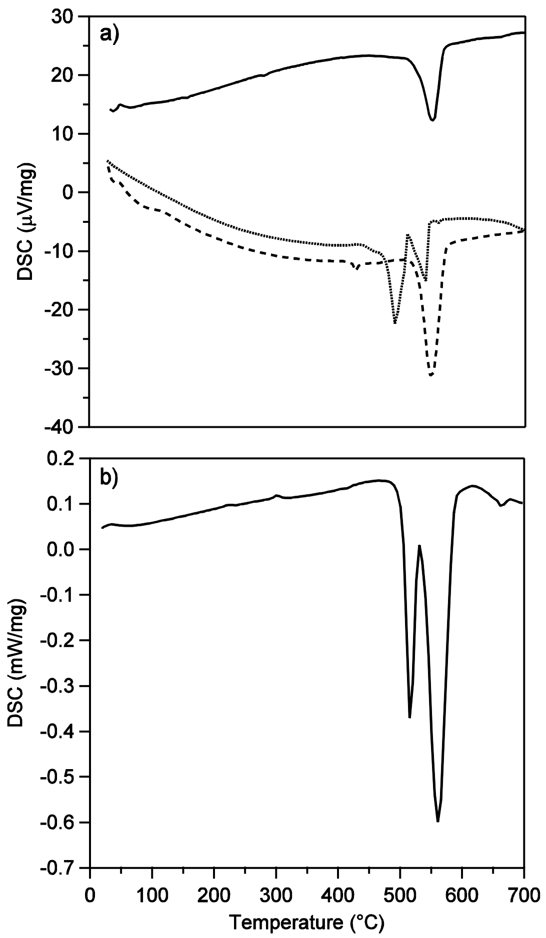

Figure S8 DSC curves of a) $NaY(IO_3)_4$ (–), $AgY(IO_3)_4$ (---) $AgBi(IO_3)_4$ (···) and b) $AgLa(IO_3)_4$.

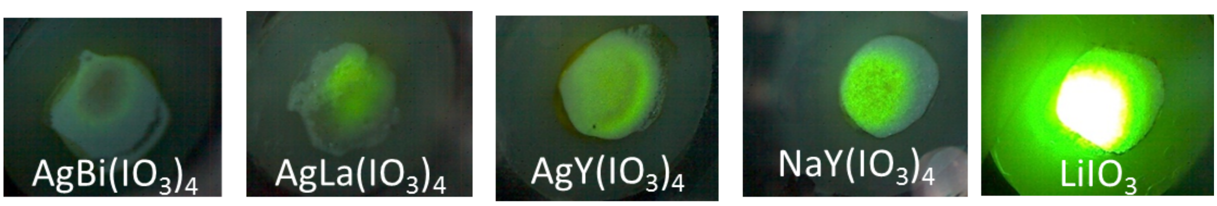

Figure S9 : Photographies showing the intensities of the emitted second harmonic generation by powders. The comparison of intensities allows us to give the followed ranking: $AgBi(IO_3)_4 < AgLa(IO_3)_4 < AgY(IO_3)_4 < NaY(IO_3)_4 < \alpha\text{-}LiIO_3$.